© 2019. Published by The Company of Biologists Ltd | Journal of Cell Science (2019) 132, jcs234237. doi:10.1242/jcs.234237

RESEARCH ARTICLE

A retention–release mechanism based on RAB11FIP2 for AMPA receptor synaptic delivery during long-term potentiation

María Royo[1,*], Yolanda Gutiérrez[1,‡], Mónica Fernández-Monreal[1,§], Silvia Gutiérrez-Eisman[1], Raquel Jiménez[1], Sandra Jurado[2] and José A. Esteban[1,¶]

ABSTRACT

It is well-established that Rab11-dependent recycling endosomes drive the activity-dependent delivery of AMPA receptors (AMPARs) into synapses during long-term potentiation (LTP). Nevertheless, the molecular basis for this specialized function of recycling endosomes is still unknown. Here, we have investigated RAB11FIP2 (FIP2 hereafter) as a potential effector of Rab11-dependent trafficking during LTP in rat hippocampal slices. Surprisingly, we found that FIP2 operates independently from Rab11 proteins, and acts as a negative regulator of AMPAR synaptic trafficking. Under basal conditions, FIP2 associates with AMPARs at immobile compartments, separately from recycling endosomes. Using shRNA-mediated knockdown, we found that FIP2 prevents GluA1 (encoded by the *Gria1* gene) AMPARs from reaching the surface of dendritic spines in the absence of neuronal stimulation. Upon induction of LTP, FIP2 is rapidly mobilized, dissociates from AMPARs and undergoes dephosphorylation. Interestingly, this dissociation of the FIP2–AMPAR complex, together with FIP2 dephosphorylation, is required for LTP, but the interaction between FIP2 and Rab11 proteins is not. Based on these results, we propose a retention–release mechanism, where FIP2 acts as a gate that restricts the trafficking of AMPARs, until LTP induction triggers their release and allows synaptic delivery.

KEY WORDS: Synaptic plasticity, Hippocampus, LTP, Membrane trafficking, Recycling endosomes

INTRODUCTION

Synaptic plasticity is widely accepted to constitute the molecular basis for learning and memory (Bliss and Collingridge, 1993). A prevalent mechanism for synaptic plasticity, in the hippocampus and other brain regions, relies on the capacity of the neuron to regulate the insertion and removal of AMPA-type glutamate receptors (AMPARs) to and from the postsynaptic membrane, in response to neuronal activity. Thus, an increase in AMPAR number at the postsynaptic membrane leads to long-term potentiation (LTP), whereas removal of receptors leads to long-term depression (LTD) (Malenka and Bear, 2004; Greger and Esteban, 2007; Kessels and Malinow, 2009; Anggono and Huganir, 2012; Herring and Nicoll, 2016). A network of Rab-driven organelles orchestrates the shuttling of receptors in and out of the synaptic membrane, across endocytic, recycling and late endosomes (Ehlers, 2000; Gerges et al., 2004; Park et al., 2004; Brown et al., 2005, 2007; Petrini et al., 2009; Fernandez-Monreal et al., 2012; Bacaj et al., 2015; Esteves da Silva et al., 2015; Mignogna et al., 2015; Gu et al., 2016).

In particular, it is now well-established that Rab11-dependent recycling endosomes drive AMPARs for synaptic delivery during plasticity events such as LTP (Brown et al., 2007; Park et al., 2004). This endosomal transport is powered by actin-based motor proteins of the myosin V family (Correia et al., 2008; Wang et al., 2008) and is also modulated by microtubule dynamics (Esteves da Silva et al., 2015). Nevertheless, it is becoming increasingly clear that recycling endosomes consist of a heterogeneous population of organelles, with distinct molecular composition and trafficking regulation, depending on their specific functions at different subcellular compartments or under different stimuli. In fact, it has been proposed that the continuous, activity-independent recycling of AMPARs in and out of the synaptic membrane involves a different population of recycling endosomes, separate from those operating during synaptic plasticity (Glebov et al., 2015; Zheng et al., 2015; but see also Petrini et al., 2009). Even the membrane fusion machinery engaged for AMPAR synaptic delivery during LTP may be different from that acting during constitutive recycling (Jurado et al., 2013) or homeostatic plasticity (Arendt et al., 2015). Therefore, it is clear that the endosomal machinery and regulatory mechanisms driving AMPARs towards synapses during LTP cannot be directly extrapolated from that of 'housekeeping' recycling endosomes, such as those typically monitored via transferrin receptors.

In this sense, we have turned our attention to the Rab11 family of interacting proteins (FIPs) as important effectors of Rab11-driven recycling endosomes, which may in principle provide functional and regulatory diversity (Hales et al., 2001). Indeed, one such effector, FIP5 (also known as RAB11FIP5), has been shown to participate in AMPAR recycling during LTD, but not during LTP or basal synaptic transmission (Bacaj et al., 2015). Another prominent member of this family, FIP2 (also known as RAB11FIP2), has been described to interact with myosin V proteins (Hales et al., 2002). Accordingly, FIP2 was proposed to link recycling endosomes with motor proteins for AMPAR mobilization and synaptic insertion upon LTP induction (Wang et al., 2008). However, this specific function of FIP2 has not been directly tested. Given the functional and molecular heterogeneity of Rab11 recycling endosomes and the specific machinery engaged for their regulation during LTP, we decided to directly evaluate the role of FIP2 in neurotransmitter receptor trafficking and synaptic function.

To this end, we used a combination of electrophysiology and fluorescence imaging, together with biochemical and molecular biology techniques, in CA1 hippocampal neurons. Surprisingly, we

[1]Department of Neurobiology, Centro de Biología Molecular 'Severo Ochoa' (CSIC-UAM), 28049 Madrid, Spain. [2]Instituto de Neurociencias CSIC-UMH, 03550 San Juan de Alicante, Spain.
*Present address: Instituto de Neurociencias CSIC-UMH, 03550 San Juan de Alicante, Spain. ‡Present address: Division of Cell Biology, Neurobiology and Biophysics, Department of Biology, Faculty of Science, Utrecht University, 3584 CH Utrecht, The Netherlands. §Present address: Bordeaux Imaging Center, Université de Bordeaux, UMS 3420 CNRS, US4 Inserm, 33000 Bordeaux, France.

¶Author for correspondence (jaesteban@cbm.csic.es)

J.A.E., 0000-0002-3759-3300

Received 10 May 2019; Accepted 15 November 2019

Journal of Cell Science (2019) 132, jcs234237. doi:10.1242/jcs.234237

found that FIP2 is not required for AMPAR synaptic delivery during LTP. Contrary to the expectation, FIP2 plays a separate, Rab11-independent function by interacting with AMPARs at extrasynaptic compartments, in this manner restricting their access to the synaptic membrane. This interaction is then released after LTP induction, which is accompanied by FIP2 dephosphorylation. Therefore, we propose a model in which FIP2 is part of a retention–release mechanism that controls AMPAR synaptic delivery during LTP.

RESULTS

FIP2 is associated with AMPARs in extrasynaptic compartments separately from recycling endosomes

FIP2 was identified as a Rab11-interacting protein that shows positive colocalization and dynamic redistribution with Rab11-containing vesicles and myosin Vb in cell lines (Hales et al., 2001; Lindsay and McCaffrey, 2002), and in primary hippocampal neurons (Wang et al., 2008). To start exploring the potential role of FIP2 in the trafficking and/or compartmentalization of AMPAR-containing endosomes, we analyzed the distribution and localization of FIP2 in relation to AMPARs and multiple intracellular membrane compartments. To this end, we expressed a GFP–FIP2 fusion protein in hippocampal primary neurons, which were then labeled with antibodies against Rab11 proteins (Rab11 hereafter), the GluA1 (encoded by the *Gria1* gene) subunit of AMPARs, and markers for different intracellular membranes (Fig. 1A,B) (immunostaining against endogenous FIP2 with commercially available antibodies was mostly non-specific, according to control experiments with our shRNA knock-down; not shown). Confocal microscopy showed that GFP–FIP2 presents a heterogeneous distribution, with widespread diffuse fluorescence and scattered clusters at perinuclear and dendritic localizations. By quantifying fluorescence correlation (Pearson's coefficients) between GFP–FIP2 and these different markers, we found that FIP2 clusters were highly colocalized with GluA1, both along dendrites and in large intracellular clusters in the cell soma (Fig. 1A, panels in first and third rows from top; quantification in Fig. 1C). Interestingly, this colocalization was much less prominent with Rab11, as a marker for recycling endosomes (Fig. 1A, panels in second and forth rows; quantification in Fig. 1C). Also, partial colocalization was observed with calnexin (endoplasmic reticulum) and EEA1 (early endosomes), and virtually absent with GM130 (cis-Golgi marker) (Fig. 1B,C). This result is consistent with a partial association of FIP2 with recycling endosomes in neurons, as previously published (Wang et al., 2008), but already suggests a distinct role for FIP2 in AMPAR trafficking and/or compartmentalization, separately from Rab11 recycling endosomes.

To investigate the dynamics of these FIP2 clusters, we carried out fluorescence recovery after photobleaching (FRAP) assays in GFP–FIP2-expressing neurons. Small regions (~1 μm^2) were chosen in both diffuse and clustered regions (Fig. 1D). Fluorescence in these regions was bleached, and images then acquired every 2 s for 2 min. These experiments showed that GFP–FIP2 clusters were fairly stable, with little fluorescence recovery throughout the time course (Fig. 1E). In contrast, diffuse GFP–FIP2 displayed virtually complete fluorescence recovery in the same time window. These results indicate that FIP2 clusters, which predominantly colocalize with AMPARs, represent immobile protein complexes.

As a complementary approach to investigate FIP2 distribution in neuronal cells, we performed sucrose gradient membrane fractionations and analyzed the presence of endogenous FIP2, Rab11 and GluA1. Whole-cell extracts were prepared from hippocampal slices, and non-synaptosomal membranes (microsomal membrane fractions) were preferentially isolated by low-speed centrifugation. These extracts were then subject to fractionation across a sucrose gradient. As shown in Fig. 1F,G, FIP2 and Rab11 segregated in very different membrane fractions, whereas fractions containing FIP2 and GluA1 were mostly overlapping.

Taken together, these results suggest that FIP2 may not be a permanent resident of Rab11 recycling endosomes in hippocampal neurons, and that it preferentially associates with AMPARs in extrasynaptic immobile compartments under basal conditions.

FIP2 restricts GluA1 surface expression on dendritic spines

In order to directly test the potential role of this extrasynaptic association between FIP2 and AMPARs, we evaluated GluA1 and GluA2 (encoded by the *Gria2* gene) subcellular distribution in neurons after knocking down endogenous FIP2. We generated a short hairpin RNA construct in a lentiviral vector to block expression of endogenous FIP2 (shFIP2). The efficiency of this construct was confirmed in cultured primary neurons after 7–10 days of infection (Fig. 1H). In addition, we tested the effectiveness of this shRNA to impair FIP2-dependent trafficking in hippocampal slice cultures. To this end, we evaluated the effect of shFIP2 on the surface expression of the transferrin receptor (TfR, encoded by the *Tfrc* gene), whose recycling to the cell membrane after endocytosis is known to depend on FIP2 function (Lindsay and McCaffrey, 2002). We co-expressed shFIP2 (or a scrambled shRNA control) with TfR tagged at the extracellular (C-terminal) end with GFP. After 7–9 days of expression, hippocampal slices were fixed and immunostained for surface TfR with an anti-GFP antibody. As shown in Fig. 2A,B, FIP2 knockdown significantly reduced the surface expression of TfR–GFP, indicating that shFIP2 can effectively impair FIP2-dependent trafficking in hippocampal slices.

To determine whether FIP2 affects AMPAR synaptic distribution, primary hippocampal neurons expressing shFIP2 (or a control scrambled shRNA) were fixed and immunostained for surface and total GluA1 or GluA2 using antibodies against N-terminal and C-terminal epitopes of these subunits. Immunofluorescence signals were then quantified along dendritic spines and neighboring dendritic shafts, and represented as spine:dendrite ratios. This approach normalizes against immunostaining variability, and evaluates the relative enrichment of AMPARs at synaptic sites. As shown in Fig. 2C, the distribution of surface GluA1 was significantly shifted towards higher spine:dendrite ratios in FIP2-depleted neurons. This result indicates an increase in surface GluA1 expression in spines in the absence of FIP2. Interestingly, this effect was only detected in surface expression, as the distribution of total (surface plus intracellular) GluA1 expression in spines and dendrites was not altered by FIP2 silencing (Fig. 2D). In addition, these changes were specific for the GluA1 subunit, as no significant change in surface or total GluA2 expression in spines was detected in FIP2 knockdown neurons (Fig. 2E,F).

Therefore, these results support the interpretation that FIP2 acts as an intracellular retention factor for AMPARs, which restricts delivery to the spine surface under basal conditions. In addition, these data point out important differences between AMPAR and TfR intracellular trafficking with respect to their dependence on FIP2.

FIP2 interacts with GluA1 and dissociates upon LTP induction, independently of Rab11 binding

Based on our colocalization results and the effect of the FIP2 knockdown, we asked whether FIP2 and GluA1 may directly interact, and whether this interaction involves Rab11. To address this question we carried out pull-down assays using extracts from hippocampal slices, and GST fusion proteins of wild-type FIP2 and two FIP2

Journal of Cell Science (2019) 132, jcs234237. doi:10.1242/jcs.234237

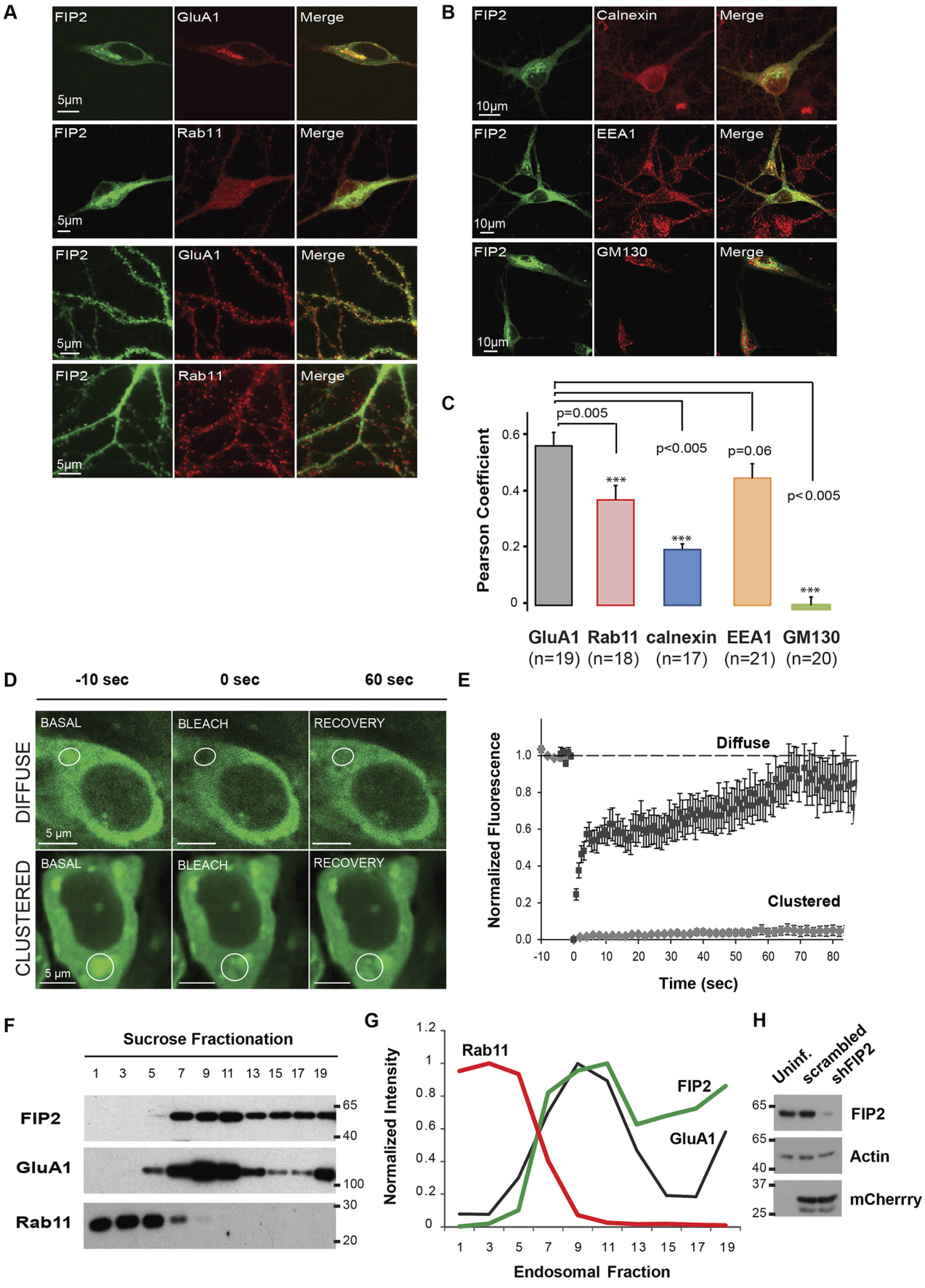

Fig. 1. See next page for legend.

Journal of Cell Science (2019) 132, jcs234237. doi:10.1242/jcs.234237

Fig. 1. FIP2 dynamics and colocalization with AMPARs and intracellular membrane markers. Efficiency of shRNA knockdown. (A,B) GFP–FIP2 was expressed for 24 h in hippocampal primary neurons. Cells were then fixed and processed for immunocytochemistry with antibodies against Rab11, GluA1 (A), or Calnexin, EEA1 or GM130 (B), as indicated. (C) Colocalization analyses were performed using Intensity Correlation Analyses (ICA, ImageJ). Mean ±s.e.m. Pearson's correlation coefficients for GFP–FIP2 clusters are plotted with respect to Rab11, GluA1, Calnexin, EEA1 and GM130. *P*-values represent statistical significance for the comparison between average Pearson's coefficients for the different markers according to the Kruskal–Wallis test ($P<0.001$) followed by Mann–Whitney post-hoc test. (D) Representative confocal images of GFP–FIP2 expression in cell somas from FRAP experiments. Images were taken under basal conditions (basal), immediately after bleaching a specific region (indicated with a white circle) (bleach), and 60 s after bleaching (recovery). Examples presented show a FRAP experiment on a diffuse GFP–FIP2 region (upper panels) and a clustered one (lower panels). (E) Quantitative analysis of FRAP experiments for diffuse (black) or clustered (gray) regions. GFP fluorescence was normalized to the fluorescence in a neighboring unbleached region, to correct for ongoing bleaching during imaging. Means±s.e.m. are plotted normalized to the baseline before bleaching. Number of regions analyzed was nine (diffuse) and five (clustered), taken from independent experiments. (F) Western blot analysis of sucrose gradient fractionation of GluA1, Rab11 and FIP2 from microsomal hippocampal membranes. Molecular mass markers are indicated on the right. (G) Quantification of GluA1, Rab11 and FIP2 abundance at different membrane fractions isolated in the sucrose gradient shown in F. (H) Western blot showing the expression levels of endogenous FIP2 in primary hippocampal neurons infected with lentivirus for the expression of shFIP2, scrambled shRNA or from uninfected neurons (control, uninf.). Molecular mass markers are indicated on the left.

mutants defective in Rab11 binding: a C-terminal truncated mutant lacking the Rab11 binding domain (GST–FIP2-ΔRBD) (Hales et al., 2001; Prekeris et al., 2001) and a point mutation in a critical residue for Rab11 binding (GST–FIP2-I481E) (Junutula et al., 2004). As shown in Fig. 3A (upper panel), GST–FIP2 was able to pull down GluA1 from hippocampal extracts. Interestingly, this interaction was independent of Rab11 binding, since both FIP2-ΔRBD and FIP2-I481E displayed effective GluA1 pull-down (in fact, both mutants appear to bind GluA1 more efficiently than the wild-type protein). As control, the inability of these mutants to bind Rab11 was also confirmed by pull-down (Fig. 3A, middle panel). To note, FIP2-ΔRBD and FIP2-I481E mutants are not necessarily equivalent. Specifically, the C-terminal coiled-coil region of FIP2 (which is partially deleted in the FIP2-ΔRBD mutant) has been shown to be involved in FIP2 homodimerization (Cullis et al., 2002; Junutula et al., 2004; Wei et al., 2006). In fact, using the GST–FIP2 pull-down, and hippocampal slices expressing GFP–FIP2 (wild type), GFP–FIP2-ΔRBD or GFP–FIP2-I481E, we have confirmed that the truncated mutant FIP2-ΔRBD cannot oligomerize with full-length GST–FIP2, whereas the point mutant FIP2-I481E can (Fig. 3B). This difference may be relevant for experiments shown below (Fig. 3E,F).

To study the FIP2–GluA1 interaction in neurons, we carried out co-immunoprecipitation assays with GFP–FIP2 expressed in hippocampal slices. As shown in Fig. 3C (left panel), we were able to detect the co-immunoprecipitation of endogenous GluA1 with GFP–FIP2 under basal conditions. To evaluate the potential regulation of this interaction during synaptic plasticity, we employed a pharmacological protocol (cLTP) that drives global neuronal bursting, resulting in robust synaptic potentiation (Otmakhov et al., 2004; Kopec et al., 2006; Arendt et al., 2014). Interestingly, the co-immunoprecipitation between FIP2 and GluA1 was significantly reduced upon cLTP induction (Fig. 3C, right panel; quantification in Fig. 3D). This result indicates that under basal conditions GluA1 and FIP2 are part of a complex and that this interaction is disrupted during LTP induction.

We have previously determined that FIP2 does not require Rab11 binding for its interaction with GluA1 (Fig. 3A). We then asked whether their dissociation induced by LTP is regulated by Rab11. We carried out similar co-immunoprecipitation experiments with the FIP2 mutants lacking Rab11 binding [see Fig. 3E for overexpression of GFP–FIP2 and its Rab11-binding mutants in slices; note that the FIP2-ΔRBD mutant is not recognized by the FIP2 antibody (top panel), but can be detected with the anti-GFP antibody (bottom panel)]. As shown in Fig. 3F, FIP2-I481E associated with GluA1 under basal conditions (as expected), and this interaction significantly decreased upon LTP induction, similar to the behavior of wild-type FIP2 (quantification in Fig. 3G). This result indicates that FIP2–GluA1 dissociation is independent of Rab11 binding. In contrast, the association of the truncated mutant, FIP2-ΔRBD, with GluA1 was present under basal conditions and was resistant to LTP induction (Fig. 3F,G). Although it is not clear why FIP2-ΔRBD does not dissociate from GluA1, it may be related to the inability of this mutant to form FIP2 dimers (Fig. 3B) (Cullis et al., 2002; Junutula et al., 2004; Wei et al., 2006).

FIP2 is redistributed within dendrites in response to LTP induction

The regulation of FIP2–AMPAR interaction during LTP induction led us to evaluate whether FIP2 subcellular distribution may also be regulated during synaptic plasticity. To test this possibility, we performed live-imaging experiments in hippocampal slices expressing GFP–FIP2, during LTP induction. When expressed in slices, GFP–FIP2 displays a predominantly diffuse, homogenous distribution in dendrites, with occasional clusters (Fig. 4A, baseline). However, we observed a dramatic redistribution in response to LTP induction, with the appearance of abundant clusters and tubule-like structures (Fig. 4A, 15′ LTP), sometimes within dendritic spines (arrows in Fig. 4A, insets). This redistribution was reversible, as GFP–FIP2 clusters gradually disappeared after LTP induction when slices were returned to normal baseline solution (Fig. 4B; quantification in Fig. 4E). To determine whether this change in FIP2 distribution requires NMDA receptor (NMDAR) activation, we performed similar live-imaging experiments in the presence of AP-V, a reversible NMDAR antagonist. As shown in Fig. 4C (two left panels), LTP induction in the presence of AP-V failed to change the pattern of GFP–FIP2 fluorescence. However, after washout of AP-V for 30 min, induction of LTP did produce dendritic clustering of FIP2 (Fig. 4C, two right panels), demonstrating that these changes are NMDAR dependent.

FIP2 has been shown to be mobilized in response to LTP induction in primary hippocampal neurons, and this movement occurs in a concerted manner with myosin Vb and recycling endosomes (Wang et al., 2008). Therefore, we tested whether LTP-induced redistribution of FIP2 in hippocampal slices requires Rab11 binding. To this end, we carried out similar live-imaging experiments with the two FIP2 mutants defective in Rab11 binding, FIP2-ΔRBD and FIP2-I481E. As shown in Fig. 4D (quantification in Fig. 4E), neither of these mutants was able to undergo redistribution into clusters upon LTP induction. This result indicates that FIP2 mobilization during LTP does require Rab11 binding, and might therefore represent enhanced recruitment of FIP2 to recycling endosomes during synaptic plasticity.

Given this dependence on Rab11 for FIP2 redistribution, we also tested its relation to myosin Vb localization. We expressed GFP–FIP2 in primary hippocampal cultures and carried out immunostaining for endogenous myosin Vb before and after LTP induction using the same pharmacological protocol we used for organotypic slices (Otmakhov et al., 2004). This protocol produced robust GFP–FIP2

Journal of Cell Science (2019) 132, jcs234237. doi:10.1242/jcs.234237

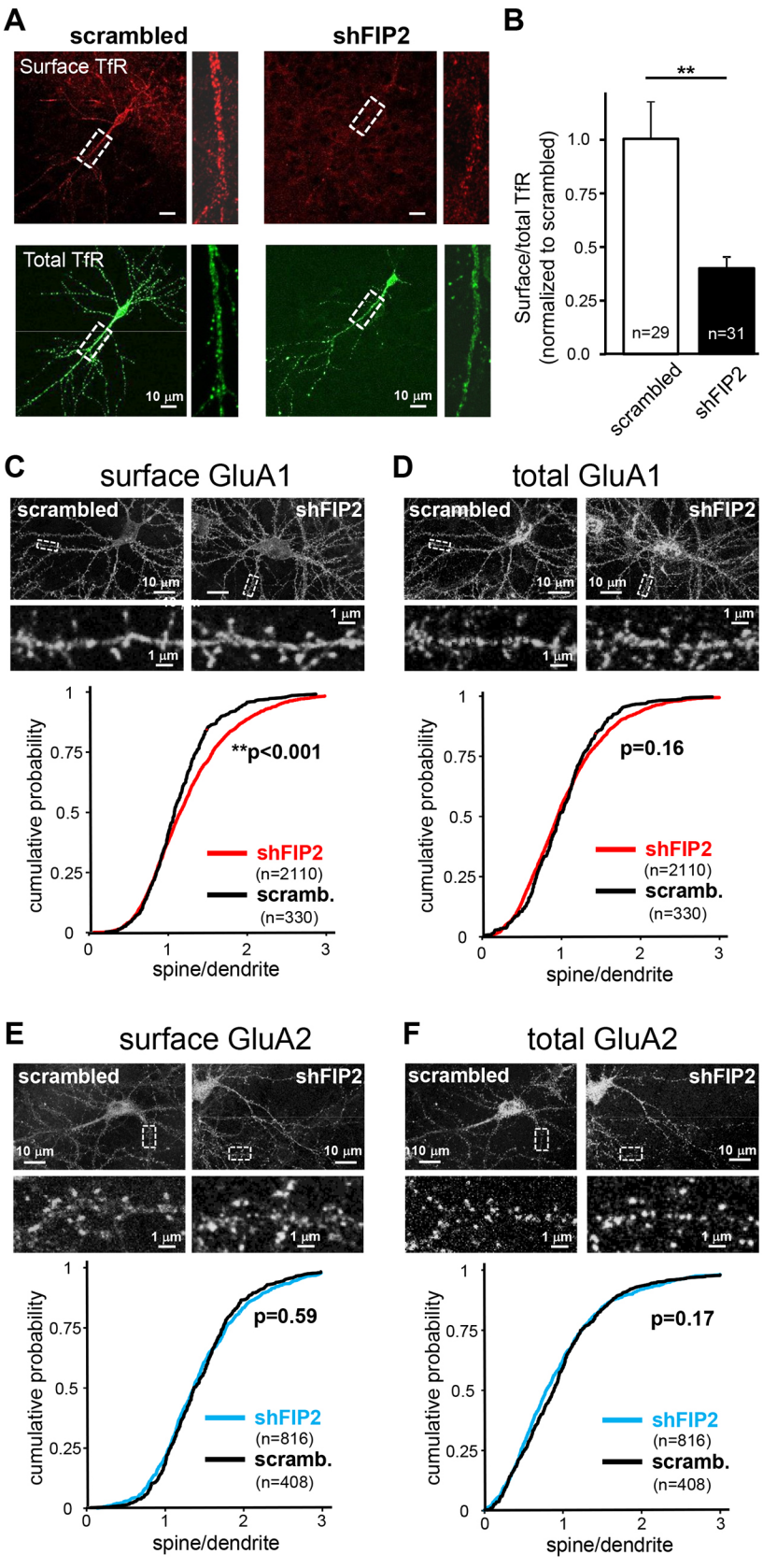

Fig. 2. FIP2 silencing decreases TfR recycling and increases GluA1 surface expression in dendritic spines. (A) Representative images of hippocampal neurons from organotypic slices expressing TfR–GFP (green channel) and shFIP2 or the scrambled shRNA control, after fixation and surface anti-GFP immunostaining (red channel). Zoomed-in regions are indicated with dashed rectangles. (B) Quantification (mean±s.e.m.) of surface TfR–GFP immunostaining signal over total TfR–GFP fluorescence, normalized to the values of scrambled shRNA. ***P*<0.001 according to the Mann–Whitney test. (C,D) Quantification of spine:dendrite ratios from immunostaining with antibodies against GluA1 N-terminus (C) or C-terminus (D) on primary hippocampal neurons expressing shFIP2 (red curves) or the scrambled control (black curves). Values are plotted as cumulative distributions. *n*, number of spines from 44 (shFIP2) or 10 (scrambled) different neurons, across four independent experiments. Statistical significance is calculated according to the Kolmogorov–Smirnov test. (E,F) Quantification of spine:dendrite ratios from immunostaining with antibodies against surface (E) and total (F) GluA2, from neurons expressing shFIP2 (blue curves) or the scrambled control (black curves). *n*, number of spines from 36 (shFIP2) or 16 (scrambled) different neurons, across four independent experiments. Statistical significance is calculated according to the Kolmogorov–Smirnov test. For C–F, representative images of neurons analyzed (upper panels) and magnified images from regions indicated with dotted boxes in upper panels (lower panels) are shown above graphs.

clustering (Fig. 4F,G; quantification in Fig. 4H), as we had observed with organotypic hippocampal slices (Fig. 4E). Interestingly, the extent of colocalization between FIP2 and myosin Vb decreased after LTP induction (Fig. 4I). These results are in contrast with those reported by Wang et al. (2008). Nevertheless, it is important to point out that this activity-dependent rearrangement of FIP2 occurs concomitantly with the dissociation of FIP2 from AMPARs (Fig. 3C,D), and consequently, it may not be associated with their

Journal of Cell Science (2019) 132, jcs234237. doi:10.1242/jcs.234237

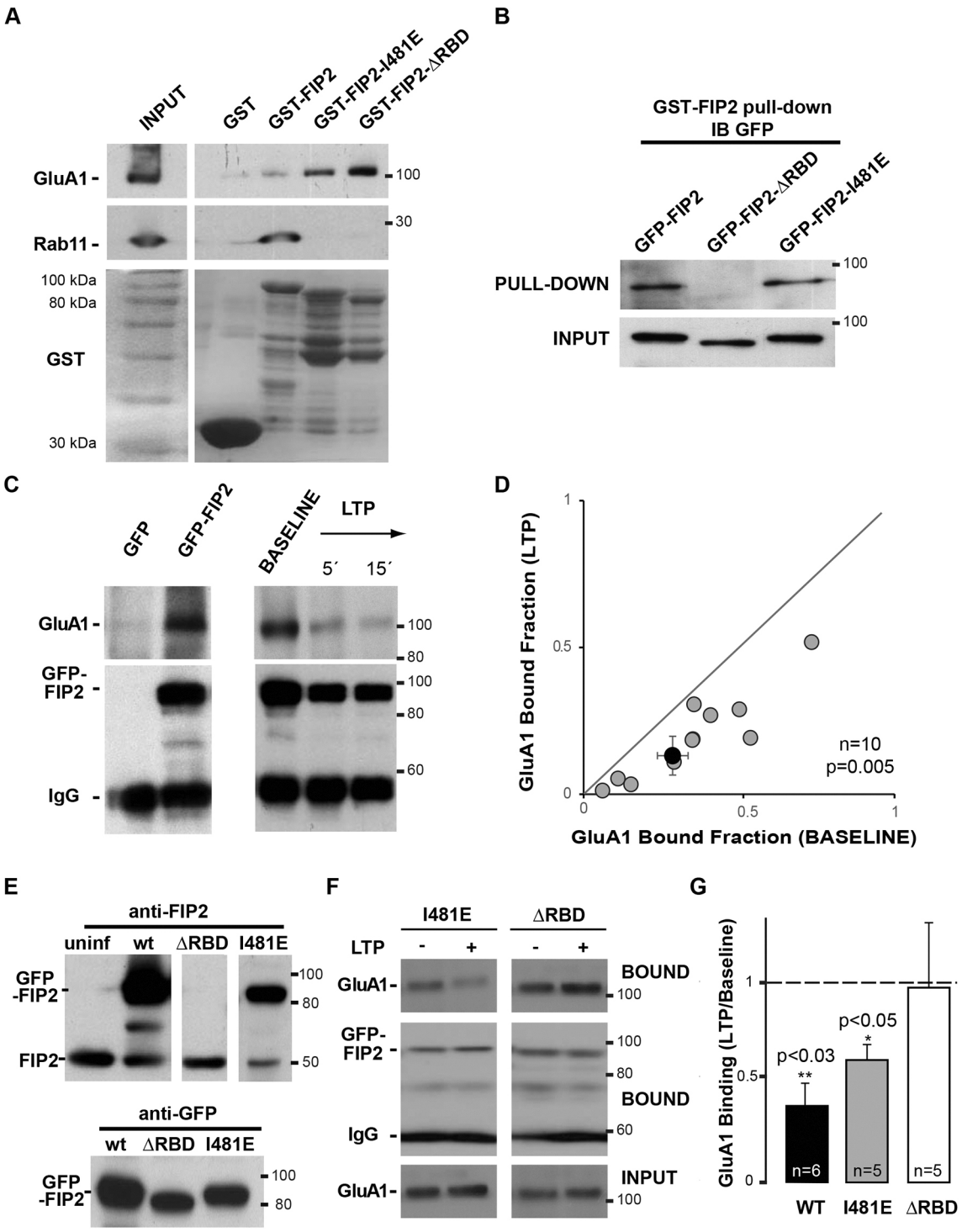

Fig. 3. See next page for legend.

myosin V-dependent trafficking. Therefore, it was important to directly test the role of FIP2 in synaptic function and LTP expression.

FIP2 is a negative regulator of LTP

To directly evaluate the role of FIP2 in synaptic potentiation during LTP, we knocked down endogenous FIP2 in CA1 pyramidal cells from rat hippocampal slice cultures using lentiviral expression of FIP2 shRNA (shFIP2). Electrophysiological recordings were carried out 7–10 days after infection. LTP was induced in infected and uninfected CA1 neurons by pairing presynaptic stimulation (3 Hz, 1.5 min) with postsynaptic depolarization (0 mV). Surprisingly, synaptic potentiation was elicited under all conditions, and was not significantly different between uninfected neurons, those expressing shFIP2, or those expressing a scrambled shRNA sequence (Fig. 5A,B). These data indicate that FIP2 is not required for LTP, and therefore, strongly suggest that FIP2 is not a necessary element to couple the trafficking machinery implicated in AMPAR transport during LTP.

Journal of Cell Science

Journal of Cell Science (2019) 132, jcs234237. doi:10.1242/jcs.234237

Fig. 3. FIP2 interacts with GluA1 independently of Rab11, and dissociates upon cLTP induction. (A) Western blot analysis of levels of GluA1 (top panel) or Rab11 (middle panel) pulled down with GST fusion proteins of full-length FIP2 (GST–FIP2) or Rab-binding domain mutants (GST–FIP2-ΔRBD and GST–FIP2-I481E), from hippocampal extracts. The expression of the corresponding GST protein was evaluated with anti-GST (bottom panel). (B) GST–FIP2 pull-down from hippocampal slices expressing GFP–FIP2 (wild-type), GFP–FIP2-ΔRBD or GFP–FIP2-I481E, as indicated. Pulled down proteins were detected using western blotting with anti-GFP antibody. (C) Left panel: co-immunoprecipitation between GFP–FIP2 and GluA1 at basal conditions. GFP-expressing slices were used as a control. Right panel: comparison of GluA1 co-immunoprecipitation at baseline and during cLTP induction, from hippocampal slices expressing GFP–FIP2. (D) Scatter-plot quantification of the fraction of GluA1 co-immunoprecipitated with GFP–FIP2 before (*x*-axis) and after (*y*-axis) cLTP treatment from 10 independent experiments. Black circle represents mean±s.e.m. Statistical significance is calculated from paired data, using the Wilcoxon test. (E) Western blot analysis of GFP–FIP2 overexpression, together with its Rab11-binding mutants (ΔRBD and I481E), in hippocampal slices. Protein expression is detected with anti-FIP2 antibody (top panel) and anti-GFP antibody (bottom panel). (F) GluA1 co-immunoprecipitation experiments as shown in C, from hippocampal slices expressing GFP–FIP2-I481E or GFP–FIP2-ΔRBD, under basal conditions and after cLTP induction (−/+LTP). (G) Quantification (mean±s.e.m.) of GluA1 co-immunoprecipitated with GFP after LTP induction, relative to the amount precipitated under basal conditions, from experiments as shown in F. *n*, number of independent experiments. *P*-values represent statistically significant difference between GluA1 co-immunoprecipitation at baseline and under LTP conditions, according to the Wilcoxon test. Molecular mass markers are indicated on the right of western blot panels.

These results came as a surprise, given the fact that FIP2 has been shown to be mobilized together with recycling endosomes and myosin V proteins during LTP (Wang et al., 2008). Nevertheless, we have observed that FIP2 interacts with AMPARs independently from recycling endosomes, and that this complex is dissociated precisely during LTP. Therefore, we decided to further explore the potential role of this interaction for synaptic potentiation. To this end, we investigated the effect on LTP of the two FIP2 mutants that cannot interact with Rab11 but display different behavior with respect to GluA1 dissociation: FIP2-I481E, which binds GluA1 and dissociates upon LTP induction (as wild-type FIP2 does), and FIP2-ΔRBD, whose binding to GluA1 persists after LTP induction (Fig. 3F,G).

We overexpressed GFP–FIP2-I481E, GFP–FIP2-ΔRBD and GFP–FIP2 (wild type) in CA1 pyramidal cells in organotypic hippocampal slices, and carried out LTP experiments as described above. We found that FIP2-I481E-expressing cells display robust LTP, similar to uninfected cells (Fig. 5C,D, orange symbols). This observation reinforces the interpretation that FIP2–Rab11 interaction is not relevant for LTP expression. Incidentally, it also serves as a control to verify that Sindbis virus infection and protein overexpression do not affect LTP. In contrast, overexpression of FIP2-ΔRBD, which is unable to dissociate from GluA1, produced a significant decrease in LTP expression, as compared to uninfected neurons (Fig. 5C,D, green symbols). This effect cannot be attributed to the inability of the mutant to bind Rab11 (according to the result with FIP2-I481E), and therefore, it is likely the consequence of its persistent binding to GluA1. Finally, the overexpression of wild-type FIP2 also reduced LTP expression (Fig. 5C,D, red symbols), perhaps due to Rab11 sequestration. Importantly, overexpression of any of these proteins did not alter basal synaptic transmission mediated by AMPARs (Fig. 5E) or NMDARs (Fig. 5F).

Taken together, these results suggest that FIP2 is a negative regulator of LTP, acting as a retention factor for AMPARs that is released by LTP induction. Interestingly, once dissociated from GluA1, FIP2 would no longer be required for AMPAR transport and synaptic potentiation.

FIP2 is phosphorylated in hippocampal slices

It has been previously shown that FIP2 phosphorylation controls intracellular membrane trafficking related to cell polarity in epithelial cell lines (Ducharme et al., 2006; Lapierre et al., 2012). Interestingly, phosphorylated FIP2 acts independently from myosin Vb and Rab11 (Lapierre et al., 2012). Therefore, we decided to investigate the role of FIP2 phosphorylation during long-term potentiation in neurons, which is known to be tightly controlled by intracellular cascades of phosphorylation and dephosphorylation (Thomas and Huganir, 2004; Lisman et al., 2012; Woolfrey and Dell'Acqua, 2015).

We first evaluated the potential of FIP2 to be phosphorylated by kinase activities present in hippocampal extracts using an *in vitro* phosphorylation assay. We overexpressed GFP–FIP2 (and GFP as a control) in CA1 pyramidal cells from organotypic hippocampal slices. Whole hippocampal extracts were prepared and incubated with [γ-^{32}P]ATP with or without Mg^{2+}. GFP–FIP2 (or the GFP control) was then immunoprecipitated with a specific anti-GFP antibody and analyzed by SDS-PAGE and autoradiography. As shown in Fig. 6A, a phosphorylated band in the expected molecular weight for GFP–FIP2 was observed only in the presence of Mg^{2+}, with no detectable signal in the absence of Mg^{2+} or in the control experiment with GFP. This result strongly suggests that FIP2 is a substrate for kinase activities present in hippocampal extracts.

Having established that FIP2 is a substrate for phosphorylation, we investigated whether FIP2 phosphorylation occurs *in situ* in hippocampal slices. We used two different approaches. First, we expressed GFP–FIP2 (and GFP as a control) in organotypic slice cultures, as described above. Whole hippocampal extracts were then prepared and immunoprecipitated with a GFP antibody. Serine phosphorylation of immunoprecipitated proteins was then analyzed by western blotting with anti-phospho-serine antibodies. As shown in Fig. 6B, a specific phospho-signal was observed in slices expressing GFP–FIP2 in the expected molecular weight, but not in GFP-expressing slices. This result indicates that FIP2 phosphorylation takes place *in situ* in hippocampal slices.

Finally, to evaluate whether endogenous FIP2 is phosphorylated in hippocampal slices, we used Phos-tag SDS-acrylamide gels. Phos-tag is a compound that binds phosphate groups in combination with metallic ions, such as zinc or manganese. During electrophoresis, Phos-tag binding to phosphorylated proteins leads to a decrease in their migration speed in comparison with non-phosphorylated ones (Kinoshita et al., 2008). Using this technique, we analyzed hippocampal slices and compared them with slices pre-treated with calyculin A, a potent inhibitor of PP1 and PP2A phosphatases (Ishihara et al., 1989). As control, some hippocampal extracts were treated *in vitro* with alkaline phosphatase (CIP) to reveal the migration position of unphosphorylated FIP2. As shown in Fig. 6C (control lanes), immunodetection with FIP2-specific antibody showed a complex phosphorylation pattern for FIP2, with at least four bands migrating above the dephosphorylated protein (CIP). This result indicates the existence of multiple phosphorylated residues on endogenous FIP2, and that most of the protein is phosphorylated to some extent under basal conditions. Importantly, this pattern of FIP2 phosphorylated bands was further shifted up upon phosphatase inhibition (calyculin A-treated slices), revealing the ongoing activity of kinases and phosphatases acting on FIP2. All these results taken together indicate that FIP2 undergoes dynamic phosphorylation and dephosphorylation in hippocampal slices under basal conditions.

Journal of Cell Science (2019) 132, jcs234237. doi:10.1242/jcs.234237

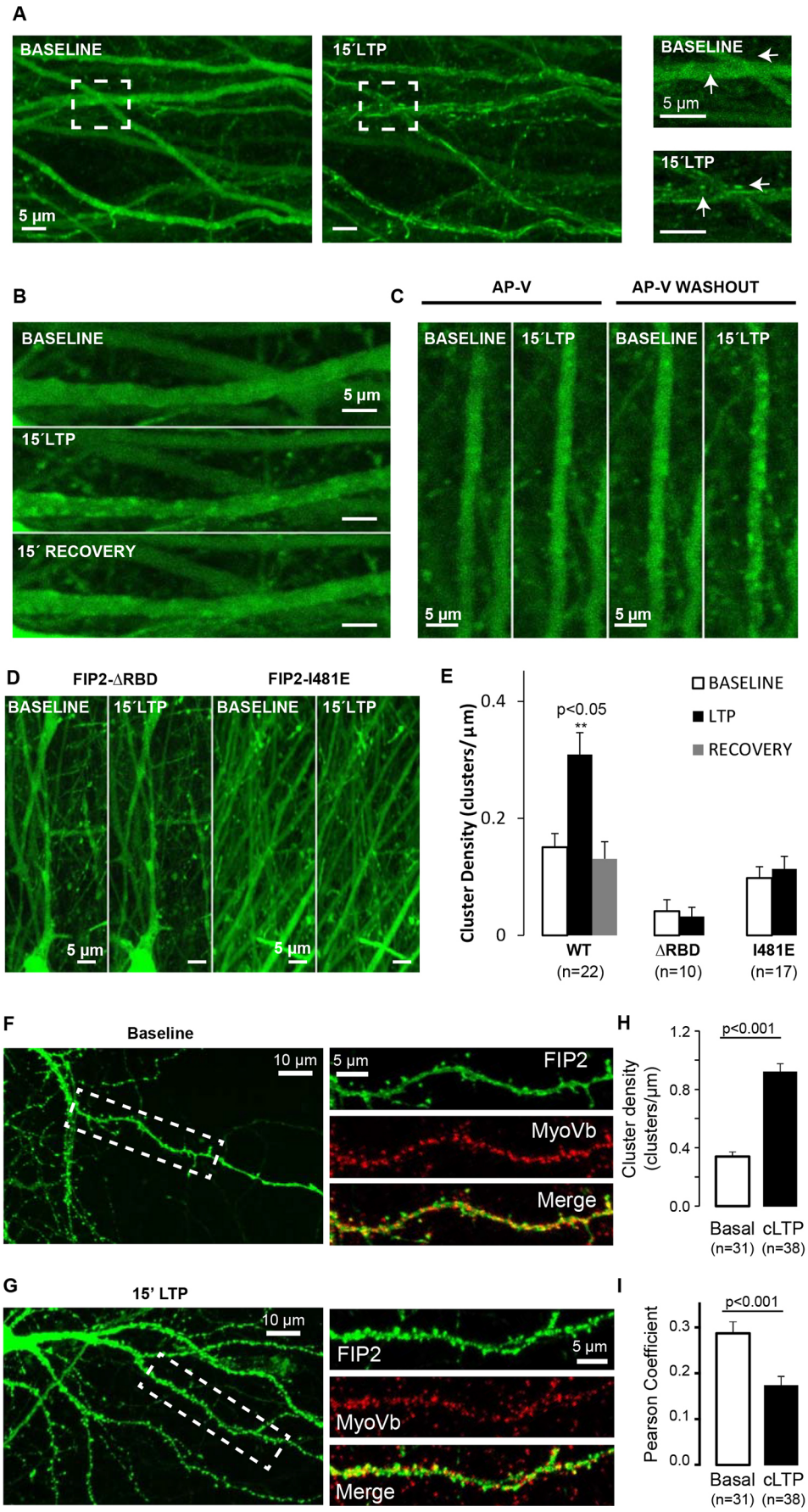

Fig. 4. Rab11- and NMDAR-dependent redistribution of GFP–FIP2 upon LTP induction. (A) Representative images of GFP–FIP2 fluorescence from dendrites of CA1 hippocampal neurons in organotypic slice cultures. Live images were acquired before (baseline) and after 15 min of cLTP induction (15′ LTP). Right panels present cropped and magnified regions showing accumulation of GFP–FIP2 in some dendritic spines (arrows). (B) Representative images showing reversible clustering of GFP–FIP2 in CA1 dendritic regions after cLTP washout (recovery). (C) Representative images of GFP–FIP2-expressing slices in presence of 0.1 mM AP-V (NMDAR antagonist). LTP-induced clustering is abolished (two left panels), and rescued after AP-V washout from the slice (two right panels). (D) Representative images of hippocampal slices expressing GFP–FIP2-ΔRBD and GFP–FIP2-I481E slices before and after 15 min of cLTP induction. (E) Quantification (mean±s.e.m.) of GFP–FIP2 cluster density from single dendrites before and after treatment. Data are taken from images as shown in A, B and D. *P*-value represents statistical significance for the comparison of GFP–FIP2 clustering before and after LTP induction, according to the Wilcoxon test. *n*, number of independent experiments. (F,G) Representative images of hippocampal primary neurons expressing GFP–FIP2 and immunostained for endogenous myosin Vb before (F) or after (G) cLTP induction. Zoomed-in regions are shown on the right panels, together with the merged GFP–FIP2 and Myosin Vb signals. (H) Quantification and statistical analysis similar to panel E, from experiments as shown in panels F and G. (I) Quantification (mean±s.e.m.) of colocalization between GFP–FIP2 and myosin Vb was carried out using intensity correlation analyses (ICA). *P*-values represent statistical significance for the comparison between mean Pearson's coefficients before and after cLTP induction according to the Mann–Whitney test. *n*, number of neurons.

Journal of Cell Science

Journal of Cell Science (2019) 132, jcs234237. doi:10.1242/jcs.234237

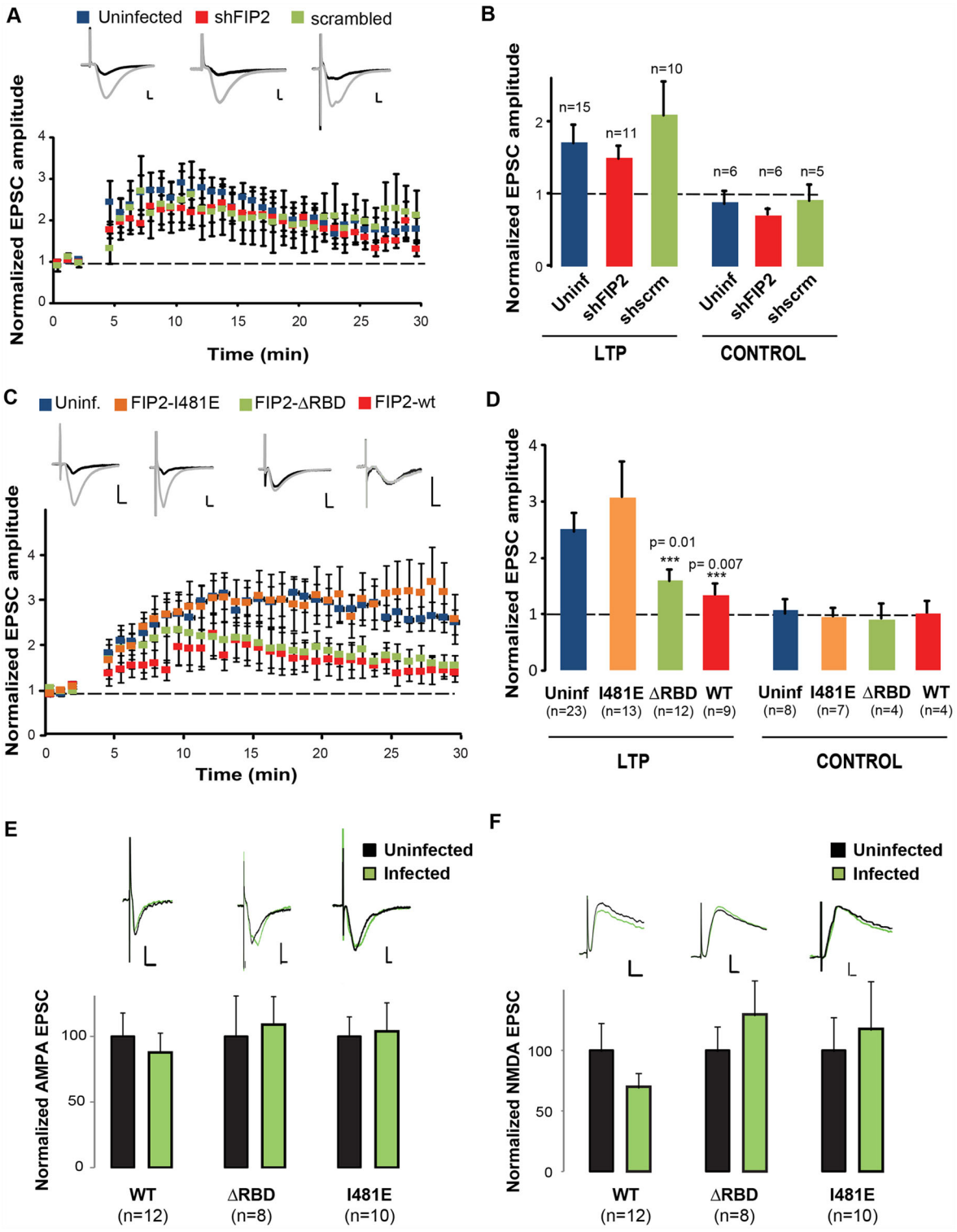

Fig. 5. See next page for legend.

FIP2 undergoes dephosphorylation during LTP induction, and serine 227 is critical for LTP expression

In order to determine whether this phosphorylation–dephosphorylation cycle of FIP2 has a role during synaptic plasticity, we evaluated changes in FIP2 phosphorylation during LTP, using the assays described above.

First, we expressed GFP–FIP2 in organotypic slices, which were then treated to induce cLTP. Phospho-FIP2 was detected using anti-GFP immunoprecipitation followed by western blotting with anti-phospho-Ser antibody (similar to Fig. 6B). As shown in Fig. 6D, there was a marked decrease in the phosphorylation of GFP–FIP2 during LTP induction (upper panel). A similar result was obtained when analyzing the phosphorylation of endogenous FIP2 using Phos-tag SDS-acrylamide gels. Upon induction of LTP, we observed a significant decrease in the highly phosphorylated forms of FIP2 (hyper-P-FIP2), and a parallel increase in the less phosphorylated

Journal of Cell Science (2019) 132, jcs234237. doi:10.1242/jcs.234237

Fig. 5. FIP2 is not required for LTP, but it is a negative regulator of LTP expression. (A) Time course of normalized AMPAR-mediated synaptic responses before and after LTP induction, from organotypic hippocampal slices expressing shFIP2 (red), scrambled shRNA (green) or from uninfected (blue) slices. Sample traces before LTP induction (black line) and 30 min after induction (gray line) are shown above the time course. Scale bars: vertical, 20 pA; horizontal, 5 ms. (B) Normalized mean±s.e.m. potentiation of AMPAR-mediated responses collected between 25 and 30 min after LTP induction from neurons expressing shFIP2, scrambled shRNA or from uninfected neurons. Paired (LTP) and unpaired (control) pathways are shown (for the unpaired pathway, the stimulating electrode is turned off during LTP induction). *n*, number of cells. (C) Time course of normalized AMPAR-mediated synaptic responses before and after LTP induction, from organotypic hippocampal slices expressing GFP–FIP2 (red), GFP–FIP2-ΔRBD (green), GFP–FIP2-I481E (orange) or uninfected controls (blue), as indicated. Scale bars of representative traces: vertical, 20 pA; horizontal, 5 ms. (D) Normalized mean±s.e.m. potentiation of AMPAR-mediated responses collected between 25 and 30 min after LTP induction from neurons as represented in C. *P*-values represent statistical significance for the comparison between uninfected and FIP2-ΔRBD, or uninfected and FIP2-WT, according to the Mann–Whitney test, after multiple-group comparison with the Kruskal–Wallis test (P=0.01). *n*, number of cells. (E,F) Mean±s.e.m. AMPAR- (E) and NMDAR- (F) mediated EPSC amplitudes (recorded at −60 mV and +40 mV, respectively) from pairs of neighboring neurons uninfected or expressing a GFP–FIP2 recombinant protein, as indicated. Scale bars of representative traces: vertical, 20 pA; horizontal, 5 ms. *n*, number of cell pairs.

forms (hypo-P-FIP2; Fig. 6E, quantification in bottom panels). To note, the reduction in the phosphorylated forms of FIP2 was statistically significant, but rather modest, probably reflecting that a limited number of phosphorylation sites are undergoing dephosphorylation during LTP. Also, these changes were reversible, as the FIP2 phosphorylation state returned to basal levels after cLTP treatment. Taken together, these two phosphorylation assays confirm that LTP induction triggers a transient dephosphorylation of FIP2.

To test the relevance of FIP2 phosphorylation and dephosphorylation during LTP, and given the complex pattern of FIP2 phosphorylation, we decided to focus on serine 227, which has already been shown to be phosphorylated in MDCK cells (Ducharme et al., 2006) and to be important for cell polarity (Lapierre et al., 2012). To this end, we designed one phospho-deficient (S227A) and two phospho-mimetic (S227D and S227E) FIP2 mutants. Also, since we have shown that Rab11 binding to FIP2 is not required for LTP (Fig. 5C,D, I481E mutant), we introduced these phosphorylation mutations in combination with I481E, in order to avoid any potential effect of Rab11 sequestration from FIP2 overexpression (Fig. 5C,D; FIP2 wild type).

We then expressed GFP–FIP2-S227A-I481E, GFP–FIP2-S227D-I481E or GFP–FIP2-S227E-I481E in CA1 pyramidal cells in organotypic hippocampal slices and we carried out LTP experiments as previously described. We found that differently from FIP2-I481E, both phospho-mimetic and phospho-deficient serine 227 mutants virtually abolished LTP, as compared to uninfected cells (Fig. 6F,G; compare with normal LTP of the FIP2-I481E mutant, Fig. 5C,D). Similar results were obtained with the single mutants GFP–FIP2-S227A and GFP–FIP2-S227D (not shown). In conclusion, these results indicate that serine 227 is critically involved in LTP. In addition, given the similar results with S227A, S227D and S227E mutants, we may speculate that a full cycle of phosphorylation and dephosphorylation of this residue is needed for LTP expression.

DISCUSSION

In this study we uncover an unexpected role of RAB11FIP2 (FIP2) as a negative regulator of AMPAR membrane trafficking during LTP. Thus, under basal conditions, FIP2 associates with AMPARs at extrasynaptic intracellular membranes separately from Rab11 recycling endosomes. This association prevents GluA1-containing AMPARs from reaching the synaptic membrane in the absence of neuronal stimulation. Then, upon LTP induction, FIP2 dissociates from AMPARs, allowing receptor engagement with Rab11-driven trafficking for synaptic delivery. At that point, FIP2 is no longer a necessary component of the AMPAR transport machinery.

Paradoxically, this function of FIP2 is independent of Rab11, despite the fact that FIP2 interacts with myosin V proteins and Rab11, two critical components of the endosomal recycling machinery mobilized during LTP (Park et al., 2004, 2006; Brown et al., 2007; Correia et al., 2008; Wang et al., 2008). Even though FIP2 has previously been identified as a Rab11-interacting protein (Hales et al., 2001) with high affinity for active, GTP-bound Rab11 (Junutula et al., 2004), there is evidence suggesting Rab11-independent functions of FIP2. First, FIP2 displays differential subcellular distributions in different cell types, with fairly complete colocalization with Rab11 in non-polarized cells (HeLa), versus partial colocalization in polarized cells, such as MDCK cells (Hales et al., 2001) or neurons (this work). Additionally, FIP2 is the only member of the Rab11-interacting protein family that contains multiple NPF motifs (Cullis et al., 2002), which allow FIP2 interactions with EH domain proteins involved in endocytosis, such as Reps1, α-adaptin (subunit of the AP-2 complex) proteins and EHD1 (Cullis et al., 2002; Naslavsky et al., 2006). Similarly, other RAB11FIPs have been described to have Rab11-independent functions, such as RAB11FIP4 (Muto et al., 2007) and RAB11FIP5 (also known as Rip11) (Welsh et al., 2007). Therefore, it is possible that FIPs generically act as scaffolding platforms that coordinate several steps within the recycling system or even the transport of different populations of recycling endosomes. In fact, there is now strong evidence for the existence of such separate populations (Kobayashi and Fukuda, 2013; Goldenring, 2015), which may differentially control the recycling of TfRs versus AMPARs (Matsuda et al., 2008). This is also consistent with the opposite behavior we have observed for the surface expression of TfRs and AMPARs upon FIP2 knockdown. Therefore, this study strengthens the notion that individual components of the recycling endosome machinery are co-opted for this functional diversity.

Another intriguing aspect of this work is the regulated dissociation of the FIP2–AMPAR complex during LTP induction, which is accompanied by reorganization of the FIP2 endosomal compartment into vesicular or tubular structures along dendrites. The association of FIP2 with AMPARs and its regulated dissociation are independent of Rab11 binding, as two different mutants unable to interact with Rab11 (FIP2-ΔRBD and FIP2-I481E) associate with AMPARs under basal conditions, and only one of them (FIP2-I481E) is able to undergo activity-dependent dissociation. In contrast, the subcellular redistribution of FIP2 during LTP induction does require Rab11 interaction, as this is absent for the two Rab11-binding mutants (FIP2-ΔRBD and FIP2-I481E). Therefore, this process probably reflects the enhanced recruitment of FIP2 into Rab11 recycling endosomes during LTP, as has been previously described (Wang et al., 2008). This clustering and tubulation of FIP2 is also reminiscent of the redistribution of the GluA1 subunit of AMPARs in response to synaptic stimulation (Shi et al., 1999). Nevertheless, at this stage FIP2 appears to act as a passive passenger, as it is no longer required for AMPAR synaptic trafficking, nor presumably for Rab11 and myosin V function. In fact, we have observed that the colocalization between FIP2 and myosin Vb decreases upon LTP induction. This is also consistent with the fact that FIP2 is dispensable for synaptic potentiation (shRNA knockdown), and expression of a Rab11-binding mutant (FIP2-I481E) does not interfere with LTP. It

Journal of Cell Science (2019) 132, jcs234237. doi:10.1242/jcs.234237

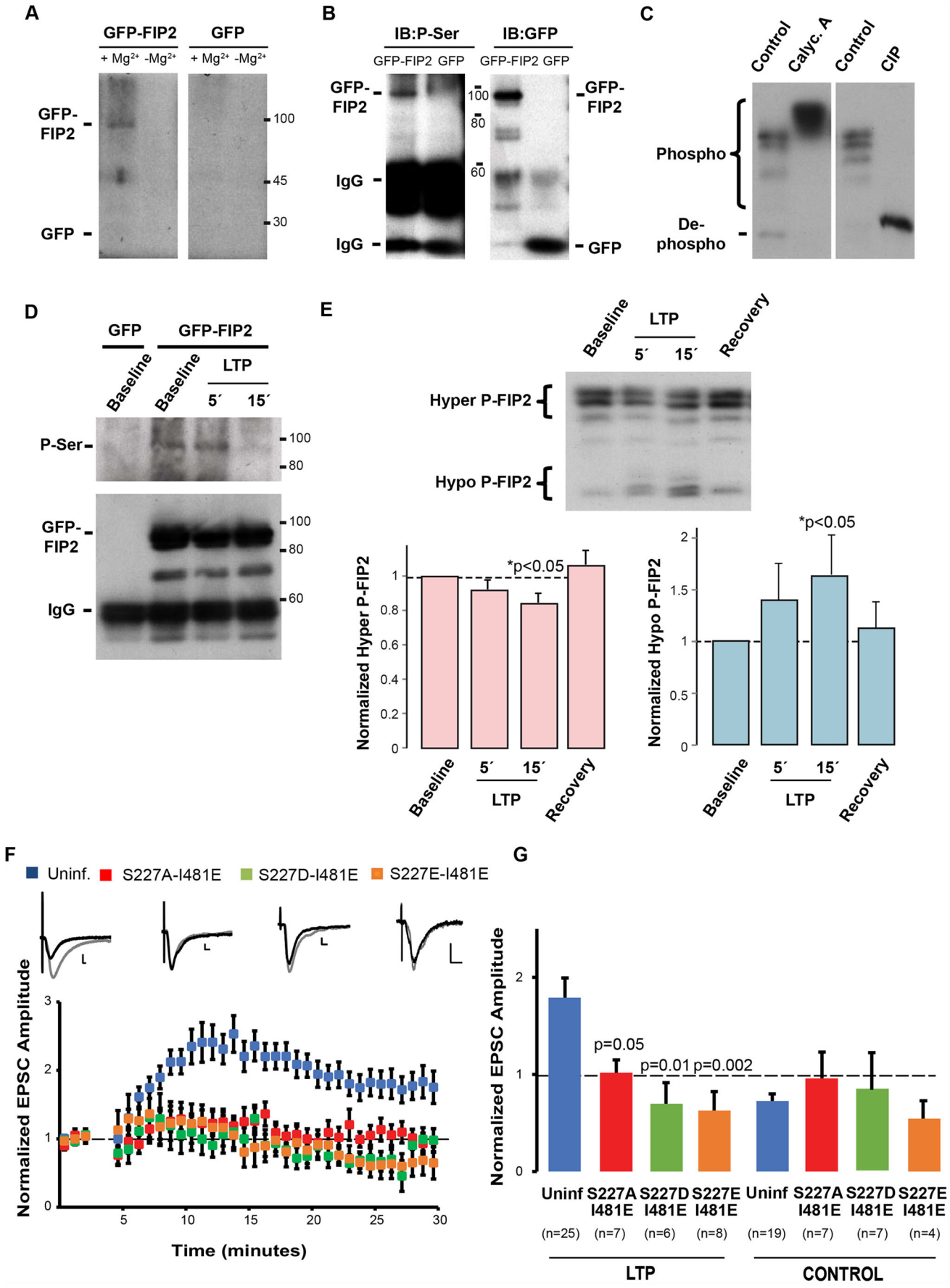

Fig. 6. See next page for legend.

Journal of Cell Science (2019) 132, jcs234237. doi:10.1242/jcs.234237

Fig. 6. Regulation of FIP2 phosphorylation during LTP, and effect of phosphorylation mutants. (A) Autoradiography analysis of protein phosphorylation from hippocampal slices expressing GFP–FIP2 or GFP. *In vitro* phosphorylation assay was carried out with [γ-^{32}P]-ATP, with or without $MgCl_2$, as indicated, followed by GFP immunoprecipitation and SDS-PAGE. Molecular mass markers are indicated on the right. (B) Western blot analysis of GFP–FIP2 phosphorylation in hippocampal slices expressing GFP–FIP2 or GFP. Recombinant proteins were isolated using anti-GFP immunoprecipitation, followed by western blotting against phospho-Ser. Molecular mass markers are indicated in between the western blot panels. (C) Phos-tag gel analysis of endogenous FIP2 phosphorylation from untreated hippocampal slices (control), or from slices treated with the PP1 and PP2A inhibitor calyculin A (Calyc. A) or dephosphorylated with calf intestinal phosphatase (CIP). (D) Western blot analysis of GFP–FIP2 phosphorylation in untreated hippocampal slices (baseline) or with slices treated to induce cLTP for 5 min (5′) or 15 min (15′), as indicated. Western blots were analyzed for expression of phospho-serine (upper panel) or GFP (lower panel; the band positions of GFP–FIP2 and the IgG used for the immunoprecipitation are indicated). Molecular mass markers are indicated on the right. (E) Phos-tag gel analysis of untreated hippocampal slices (baseline) or slices treated for cLTP induction for 5 min or 15 min, or recovered in baseline solution for 15 min after cLTP induction, as indicated. Higher phosphorylated forms of FIP2 (upper bands) are referred to as hyper-P-FIP2, and less phosphorylated forms (lower bands) as hypo-P-FIP2. Graph below shows quantification mean±s.e.m. of the amount of hyper- or hypo-phosphorylated FIP2 normalized to baseline, from seven independent experiments as shown in the upper panel. *P*-values represent statistical significance for the comparison between the phosphorylation state of FIP2 before (baseline) and after LTP induction (15 min) according to the Wilcoxon test. (F) Time course of normalized AMPAR-mediated synaptic responses before and after LTP induction, from organotypic slices expressing GFP–FIP2-S227A-I481E (red), GFP–FIP2-S227D-I481E (green), GFP–FIP2-S227E-I481E (orange) or from uninfected (blue) slices. Sample traces before LTP induction (black line) and 30 min after induction (gray line) are shown above the time course. Scale bars: vertical, 10 pA; horizontal, 10 ms. (G) Normalized mean±s.e.m. potentiation of AMPAR-mediated responses collected between 25 and 30 min after LTP induction from neurons expressing GFP–FIP2-S227A-I481E (red), GFP–FIP2-S227D-I481E (green), GFP–FIP2-S227E-I481E (orange) or from uninfected neurons (blue). Paired (LTP) and unpaired (control) pathways are shown (for the unpaired pathway, the stimulating electrode is turned off during LTP induction). *P*-values represent statistical significance for the comparison between uninfected and each of the FIP2 mutations according to the Mann–Whitney test, after multiple-group comparison with the Kruskal–Wallis test (P=0.007). *n*, number of cells.

remains to be determined whether an alternative RAB11FIP family member is required to regulate Rab11-dependent trafficking during LTP. If this is the case, it should also be different from RAB11FIP5 (Bacaj et al., 2015).

In contrast to Rab11 binding, the ability of FIP2 to interact with AMPARs does have a direct impact on LTP. In fact, FIP2–AMPAR dissociation appears to be a limiting factor for synaptic potentiation. Thus, increasing FIP2 levels or expressing a mutant FIP2 unable to dissociate from AMPARs impairs LTP. The molecular basis for the FIP2–AMPAR association and release are unknown, but it is intriguing that the truncated mutant FIP2-ΔRBD, which cannot dimerize (Cullis et al., 2002; Junutula et al., 2004; Wei et al., 2006), is also unable to dissociate from AMPARs. It is therefore tempting to speculate that FIP2 associates with AMPARs as a monomer under basal conditions, and dimerization is required to dissociate the FIP2–AMPAR complex.

In addition, we have observed that AMPAR dissociation is accompanied by FIP2 dephosphorylation. FIP2 displays a complex pattern of phosphorylation in hippocampal neurons, which likely involves multiple phosphorylation sites. Nevertheless, phosphorylation of FIP2 at serine 227 has already been shown to regulate FIP2-dependent membrane trafficking (Ducharme et al., 2006), interestingly, in a myosin Vb- and Rab11-independent manner (Lapierre et al., 2012). We now show that phosphorylation–dephosphorylation events at serine 227 appear to be involved in LTP, as both phospho-mimetic (S227D, S227E) and phospho-deficient (S227A) FIP2 mutants abolished LTP expression. Undoubtedly, further work will be required to identify the kinases and phosphatases involved, as well as their potential regulation during synaptic plasticity.

In summary, this work has defined a newly identified retention–release mechanism for the synaptic delivery of AMPARs during LTP, and highlights the complexity and specialization of the endosomal transport machinery for synaptic trafficking.

MATERIALS AND METHODS

Neuronal cultures, expression of recombinant proteins and antibodies

All the biosafety procedures for handling and euthanasia of animals were approved by the bioethics committee of the Consejo Superior de Investigaciones Cientificas (CSIC), and followed the European Commission guidelines for the welfare of experimental animals (2010/63/EU, 86/609/EEC).

Organotypic hippocampal slice cultures were prepared as previously described (Gähwiler et al., 1997). In brief, hippocampal slices are prepared from young rats (Wistar, postnatal days 5–7; provided by Charles River) of either sex, placed in culture on permeable membranes in a medium containing 20% horse serum, 1 mM L-glutamine, 1 mM $CaCl_2$, 2 mM $MgSO_4$, 1 mgl^{-1} insulin, 0.0012% ascorbic acid, 30 mM HEPES, 13 mM D-glucose and 5.2 mM $NaHCO_3$, and maintained at 35.5°C. Culture medium was replaced with fresh medium every 2–3 days. The slices were used after 7–10 days *in vitro*. For primary hippocampal neurons, hippocampi were dissected from embryonic day (E)18 rat embryos and cells dissociated with trypsin. Neurons were plated onto poly-L-lysine-coated coverslips and cultured in Neurobasal medium supplemented with B27 (GIBCO, 17504044) and L-glutamine (GIBCO, 25030024). Cells were maintained at 37°C and 5% CO_2.

Rat FIP2 (RAB11FIP2) full-length cDNA was cloned into pEGFP-C1 (Clontech) by in-frame ligation of the EGFP coding sequence with the N-terminus of FIP2. GFP–FIP2-ΔRBD (deletion of the C-terminal 56 amino acids of FIP2), GFP–FIP2-I481E, GFP–FIP2-S227A-I481E, GFP–FIP2-S227E-I481E and GFP–FIP2-S227D-I481E mutants were generated by PCR site-directed mutagenesis. All constructs were prepared in pSinRep5 for expression using Sindbis virus (Malinow et al., 2010). Recombinant proteins were expressed in hippocampal CA1 pyramidal neurons from organotypic slice cultures or in hippocampal primary neurons for 24 h.

The shRNA sequence specific for FIP2 was 5′-GGAACAACATGACAG-CAAGCA-3′. Two complementary oligonucleotides with this target sequence were annealed and cloned into the KH1-LV vector (provided by the laboratory of María S. Soengas, Madrid, Spain), which also expresses mCherry under the control of the ubiquitin promoter. A scrambled shRNA sequence (5′-GGA-ACGAACCCAGCAAGAATA-3′) was used as negative control. These vectors were transfected into 293T cells (ATCC, CRL-3216™), together with packaging plasmids pCMVdR8.74 (#22036, Addgene) and pMD2G (#12259, Addgene). Viral supernatants were collected 48 h after transfection and frozen in individual aliquots at −80°C. shRNA constructs were expressed in hippocampal slices or hippocampal primary neurons for 7–10 days.

Antibodies against the following were used: GluA1 N-terminus (Millipore, MAB2263, clone RH95), GluA1 C-terminus (Abcam, AB31232), GluA2 N-terminus (Millipore, MAB397, clone 6C4), GluA2 C-terminus (Neuromab, 75-002), RAB11FIP2 (Abcam, ab76892), GFP (Roche, 11814460001), Rab11 (BD Biosciences, 610656), calnexin (StressMarq Biosciences, SPC-108), EEA1 (Santa Cruz Biotechnology, sc-6415), GM130 (BD Biosciences, 610823), myosin Vb (Novus Biologicals, NBP1-87746) and phospho-serine (cocktail of six phospho-specific antibodies; Nanotools, 0701). All primary antibodies were used at 1:100 dilution for immunocytochemistry and 1:1000 dilution for western blotting. Secondary antibodies for western blotting were from Jackson Immunoresearch (anti-mouse-Ig and anti-rabbit-Ig antibodies coupled to horseradish peroxidase; 715-035-151 and 711-035-152, respectively; 1:10,000 dilution). Antibodies were validated by the commercial supplier.

Live imaging in hippocampal slices

Organotypic hippocampal slices were maintained under perfusion with artificial cerebrospinal fluid (ACSF) containing 119 mM NaCl, 2.5 mM KCl, 4 mM

$CaCl_2$, 4 mM $MgCl_2$, 26 mM $NaHCO_3$, 1 mM NaH_2PO_4, 11 mM glucose, 0.1 mM picrotoxin and 4 µM 2-chloroadenosine, pH 7.4, gassed with 5% CO_2 and 95% O_2 at 29°C. *Z*-stack confocal fluorescence images were obtained with an LSM510 Zeiss microscope and analyzed with ImageJ software.

Surface immunostaining of recombinant TfR–EGFP

Organotypic slice cultures were transfected with a biolistic delivery method at 1 day *in-vitro* (DIV1) and maintained for 7–9 days before fixation with 4% paraformaldehyde. Immunohistochemistry of surface GFP was performed under non-permeabilizing conditions with anti-GFP antibody, followed by incubation with anti-mouse-Ig secondary antibody coupled to Alexa Fluor 594 (Invitrogen, A-21203; 1:1000 dilution). Quantifications were performed using ImageJ software, defining a mask for the whole neuron on the total TfR–GFP channel, and measuring intensity both in the total (GFP) and surface (immunolabeling) TfR channels. All fluorescence intensities were normalized to the surface:total ratio of neurons expressing scrambled shRNA.

Immunostaining of primary hippocampal neurons

Neuronal cultures were fixed with 4% paraformaldehyde and immunostained with the indicated antibodies. For surface immunostaining, neurons were incubated without permeabilization with the antibody against GluA1 or GluA2 N-terminus, and anti-mouse-Ig secondary antibodies coupled to Alexa Fluor 594 (Invitrogen, A-21203, 1:1000 dilution). Afterwards, neurons were permeabilized with 0.3% Triton X-100 in blocking solution [1% bovine serum albumin (Sigma, A4503) 0.2% fish gelatin (Sigma, G7765) in phosphate buffered saline], followed by incubation with antibodies against GluA1 or GluA2 C-terminus, and anti-rabbit-Ig secondary antibodies coupled to Alexa Fluor 647 (Invitrogen, A-31573; 1:1000 dilution). For myosin Vb immunostaining after LTP induction, cells were fixed for 5 min in 3% paraformaldehyde immediately following treatment under cLTP or baseline conditions (according to the experimental condition). To preserve FIP2 clusters, permeabilization was performed with 0.1% saponin for 10 min and blocking with 3% BSA for 10 min, with extensive PBS washes in between. Quantifications were carried out with ImageJ software. Regions of interest corresponding to individual spines and dendrites were manually selected. All fluorescence intensities were corrected for background labeling. Pearson's correlation coefficients were calculated with the Intensity Correlation Analysis plugin of Image J.

Electrophysiology

The recording chamber was perfused with ACSF, gassed with 5% CO_2 and 95% O_2. Patch recording pipettes (3–6 MΩ) were filled with 115 mM Cs methanesulfonate, 20 mM CsCl, 10 mM HEPES, 2.5 mM $MgCl_2$, 4 mM Na_2ATP, 0.4 mM Na_3GTP, 10 mM Na phosphocreatine and 0.6 mM EGTA, pH 7.25. Synaptic responses were evoked with bipolar electrodes using single-voltage pulses (200 µs, up to 20 V). LTP was induced using a pairing protocol by stimulating Schaffer collateral fibers at 3 Hz (300 pulses) while depolarizing the postsynaptic cell to 0 mV. Only CA1 cells (and not CA3 cells) were infected with viral vectors; this configuration ensures that recombinant proteins or shRNAs are expressed exclusively in the postsynaptic cell.

Pharmacological treatments, immunoprecipitations and pull-downs

For chemical LTP treatment (cLTP), hippocampal slices were transferred to a submersion-type holding chamber containing ACSF, gassed with 5% CO_2 and 95% O_2. Slices were equilibrated in the holding chamber for 5 min before each experiment and were transferred to a separate chamber with modified ACSF, lacking $MgCl_2$ and containing 0.1 µM rolipram, 50 µM forskolin and 100 µM picrotoxin (Otmakhov et al., 2004). The slices remained in this solution between 5 and 15 min, as indicated in each experiment. For some experiments, slices were then returned to regular ACSF (recovery). To prepare hippocampal extracts, slices were homogenized in a buffer containing 50 mM Tris-HCl, 150 mM NaCl, 1 mM EDTA, 1% Triton X-100 (v/v), and a protease inhibitor cocktail (Complete EDTA-free, Roche).

For immunoprecipitation experiments, 150–300 µg of protein extracts were incubated with anti-GFP antibody (Roche, 11814460001; 2 µg) and with 40 µl of protein G–sepharose beads (50%) (Amersham Biosciences) for 2 h at 4°C. These samples were then washed and immunoprecipitated proteins were eluted by boiling in 1× Laemmli sample buffer (62.5 mM Tris-HCl, 2% SDS, 10% glycerol, 0.625% β-mercaptoethanol) and separated by SDS–PAGE.

For GST pull-down experiments, hippocampi were homogenized in a lysis buffer containing 10 mM HEPES pH 7.4, 150 mM NaCl, 5 mM $MgCl_2$, 1% Triton X-100, 5% glycerol and a protease inhibitor cocktail (Complete EDTA-free, Roche). 100–500 µg of soluble extracts were incubated with glutathione–Sepharose 4B (Amersham Pharmacia Biotech) coupled to GST or GST-fusion for 1 h at 4°C, followed by four washes in PBS (0.1% Triton X-100). These samples were then washed, and proteins were eluted by boiling in 1× Laemmli sample buffer and separated by SDS-PAGE.

Visualization of immunoprecipitated and pulled down proteins was performed by western blotting, developed with chemiluminescence and quantified with ImageJ under linear conditions.

FIP2 phosphorylation assays

In-vitro phosphorylation

Hippocampal organotypic slices (5–7 days in culture) were homogenized in the same buffer as described above for pharmacological treatments (chemical LTP), without EDTA. We used ∼200 µg of total protein in a final volume of 100 µl. Reactions were started with the addition of 10 µM ATP, [γ-^{32}P]-ATP (50 µCu/µl) and 5 mM $MgCl_2$. 10 mM EDTA was added to the negative controls (−Mg^{2+}). Samples were incubated for 30 min at 30° C, and analyzed by immunoprecipitation with anti-GFP antibody and electrophoresis on regular 8–12% acrylamide gels (SDS-PAGE) for protein separation. Phosphorylated substrates were visualized using standard autoradiography.

Phostag gels

Standard 8–12% SDS-PAGE gels were premixed with 50 µM Phos-tag (Wako Phos-tag Acrylamide AAL-107) and 200 µM $MnCl_2$. After electrophoresis, gels were incubated for 30 min in standard transfer buffer containing 10 mM EDTA for the complete washout of Mn^{2+}. Visualization of proteins was performed using western blotting with an antibody to RAB11FIP2 and secondary antibody as described above.

Membrane fractionation in sucrose gradient

Membrane fractionations were carried out as previously described (Arendt et al., 2014). Briefly, hippocampal slices were mechanically homogenized in a buffer containing 10% sucrose, 10 mM HEPES (pH 7.4), and a cocktail of protease inhibitors from Roche (Complete Mini EDTA-free). Protein extracts were spun down at 1400 ***g*** for 10 min at 4°C to remove nuclei and cell debris. The supernatant was spun down at 11,600 ***g*** for 10 min at 4°C. The pellet (crude synaptosomal fraction) was discarded. The supernatant (microsomal fraction), containing 10% sucrose, was loaded on top of a discontinuous sucrose gradient, in 10 mM HEPES (pH 7.4), containing layers of 15%, 20%, 25%, 30%, 35%, 40% and 45% sucrose (from top to bottom), each layer with a volume of 200 µl. The gradient was spun down at 62,000 ***g*** for 6 h at 4°C. Fractions of 100 µl were collected from top to bottom, and analyzed by SDS-PAGE and western blotting with antibodies specific to GluA1, Rab11 and FIP2, and secondary antibodies as described above.

Statistical analyses

All graphs represent mean±s.e.m. Statistical differences were calculated according to nonparametric tests. For comparisons with multiple groups, the Kruskall–Wallis test was followed by post-hoc Mann–Whitney tests. *P*-values for pairwise comparisons were calculated according to two-tailed Mann–Whitney tests (for unpaired data), or Wilcoxon's tests (for paired data). Cumulative probability distributions were compared with Kolmogorov–Smirnov tests.

Acknowledgements

We thank Daniel Choquet for generously providing the pBA-TfR-EGFP plasmid for the expression of the GFP-tagged transferrin receptor. We thank María Muñoz for the preparation of specific DNA constructs for protein expression, Sergio López for providing organotypic slice cultures, and the personnel at the fluorescence microscopy facility of the CBMSO (SMOC) for their expert technical assistance. We

also thank members of the Esteban laboratory for their critical reading of the manuscript.

Competing interests
The authors declare no competing or financial interests.

Author contributions
Conceptualization: M.R., Y.G., M.F.-M., J.A.E.; Methodology: M.R., Y.G., M.F.-M., S.G.-E., R.J., J.A.E.; Formal analysis: M.R., Y.G., M.F.-M., J.A.E.; Investigation: M.R., Y.G., M.F.-M.; Resources: S.J., J.A.E.; Writing - original draft: M.R.; Writing - review & editing: Y.G., J.A.E.; Supervision: J.A.E.; Project administration: J.A.E.; Funding acquisition: J.A.E.

Funding
This work was supported by grants from the Ministerio de Ciencia, Innovación y Universidades (Spanish Ministry of Science, Innovation and Universities) (SAF2015-72988-EXP, SAF2017-86983-R) and the European Union Joint Programming Initiative A healthy diet for a healthy life (PCIN-2016-095). M.R. and Y.G. were recipients of pre-doctoral contracts from the Instituto de Salud Carlos III and from the Ministerio de Educación, Cultura y Deporte (Spanish Ministry of Education, Culture and Sport), respectively. M.F.-M. was supported by the International Reintegration Grant program from the European Commission (MC-IRG268446).

References
Anggono, V. and Huganir, R. L. (2012). Regulation of AMPA receptor trafficking and synaptic plasticity. *Curr. Opin. Neurobiol.* **22**, 461-469. doi:10.1016/j.conb.2011.12.006

Arendt, K. L., Benoist, M., Lario, A., Draffin, J. E., Munoz, M. and Esteban, J. A. (2014). PTEN counteracts PIP3 upregulation in spines during NMDA-receptor-dependent long-term depression. *J. Cell Sci.* **127**, 5253-5260. doi:10.1242/jcs.156554

Arendt, K. L., Zhang, Y., Jurado, S., Malenka, R. C., Südhof, T. C. and Chen, L. (2015). Retinoic acid and LTP recruit postsynaptic AMPA receptors using distinct SNARE-dependent mechanisms. *Neuron* **86**, 442-456. doi:10.1016/j.neuron.2015.03.009

Bacaj, T., Ahmad, M., Jurado, S., Malenka, R. C. and Südhof, T. C. (2015). Synaptic function of Rab11Fip5: selective requirement for hippocampal long-term depression. *J. Neurosci.* **35**, 7460-7474. doi:10.1523/JNEUROSCI.1581-14.2015

Bliss, T. V. P. and Collingridge, G. L. (1993). A synaptic model of memory: long-term potentiation in the hippocampus. *Nature* **361**, 31-39. doi:10.1038/361031a0

Brown, T. C., Tran, I. C., Backos, D. S. and Esteban, J. A. (2005). NMDA receptor-dependent activation of the small GTPase Rab5 drives the removal of synaptic AMPA receptors during hippocampal LTD. *Neuron* **45**, 81-94. doi:10.1016/j.neuron.2004.12.023

Brown, T. C., Correia, S. S., Petrok, C. N. and Esteban, J. A. (2007). Functional compartmentalization of endosomal trafficking for the synaptic delivery of AMPA receptors during long-term potentiation. *J. Neurosci.* **27**, 13311-13315. doi:10.1523/JNEUROSCI.4258-07.2007

Correia, S. S., Bassani, S., Brown, T. C., Lisé, M.-F., Backos, D. S., El-Husseini, A., Passafaro, M. and Esteban, J. A. (2008). Motor protein-dependent transport of AMPA receptors into spines during long-term potentiation. *Nat. Neurosci.* **11**, 457-466. doi:10.1038/nn2063

Cullis, D. N., Philip, B., Baleja, J. D. and Feig, L. A. (2002). Rab11-FIP2, an adaptor protein connecting cellular components involved in internalization and recycling of epidermal growth factor receptors. *J. Biol. Chem.* **277**, 49158-49166. doi:10.1074/jbc.M206316200

Ducharme, N. A., Hales, C. M., Lapierre, L. A., Ham, A. J., Oztan, A., Apodaca, G. and Goldenring, J. R. (2006). MARK2/EMK1/Par-1Balpha phosphorylation of Rab11-family interacting protein 2 is necessary for the timely establishment of polarity in Madin-Darby canine kidney cells. *Mol. Biol. Cell* **17**, 3625-3637. doi:10.1091/mbc.e05-08-0736

Ehlers, M. D. (2000). Reinsertion or degradation of AMPA receptors determined by activity-dependent endocytic sorting. *Neuron* **28**, 511-525. doi:10.1016/S0896-6273(00)00129-X

Esteves da Silva, M., Adrian, M., Schätzle, P., Lipka, J., Watanabe, T., Cho, S., Futai, K., Wierenga, C. J., Kapitein, L. C. and Hoogenraad, C. C. (2015). Positioning of AMPA receptor-containing endosomes regulates synapse architecture. *Cell Reports* **13**, 933-943. doi:10.1016/j.celrep.2015.09.062

Fernandez-Monreal, M., Brown, T. C., Royo, M. and Esteban, J. A. (2012). The balance between receptor recycling and trafficking toward lysosomes determines synaptic strength during long-term depression. *J. Neurosci.* **32**, 13200-13205. doi:10.1523/JNEUROSCI.0061-12.2012

Gähwiler, B. H., Capogna, M., Debanne, D., McKinney, R. A. and Thompson, S. M. (1997). Organotypic slice cultures: a technique has come of age. *Trends Neurosci.* **20**, 471-477. doi:10.1016/S0166-2236(97)01122-3

Gerges, N. Z., Backos, D. S. and Esteban, J. A. (2004). Local control of AMPA receptor trafficking at the postsynaptic terminal by a small GTPase of the Rab family. *J. Biol. Chem.* **279**, 43870-43878. doi:10.1074/jbc.M404982200

Glebov, O. O., Tigaret, C. M., Mellor, J. R. and Henley, J. M. (2015). Clathrin-independent trafficking of AMPA receptors. *J. Neurosci.* **35**, 4830-4836. doi:10.1523/JNEUROSCI.3571-14.2015

Goldenring, J. R. (2015). Recycling endosomes. *Curr. Opin. Cell Biol.* **35**, 117-122. doi:10.1016/j.ceb.2015.04.018

Greger, I. H. and Esteban, J. A. (2007). AMPA receptor biogenesis and trafficking. *Curr. Opin. Neurobiol.* **17**, 289-297. doi:10.1016/j.conb.2007.04.007

Gu, Y., Chiu, S.-L., Liu, B., Wu, P.-H., Delannoy, M., Lin, D.-T., Wirtz, D. and Huganir, R. L. (2016). Differential vesicular sorting of AMPA and GABAA receptors. *Proc. Natl. Acad. Sci. USA* **113**, E922-E931. doi:10.1073/pnas.1525726113

Hales, C. M., Griner, R., Hobdy-Henderson, K. C., Dorn, M. C., Hardy, D., Kumar, R., Navarre, J., Chan, E. K., Lapierre, L. A. and Goldenring, J. R. (2001). Identification and characterization of a family of Rab11-interacting proteins. *J. Biol. Chem.* **276**, 39067-39075. doi:10.1074/jbc.M104831200

Hales, C. M., Vaerman, J. P. and Goldenring, J. R. (2002). Rab11 family interacting protein 2 associates with Myosin Vb and regulates plasma membrane recycling. *J. Biol. Chem.* **277**, 50415-50421. doi:10.1074/jbc.M209270200

Herring, B. E. and Nicoll, R. A. (2016). Long-term potentiation: from CaMKII to AMPA receptor trafficking. *Annu. Rev. Physiol.* **78**, 351-365. doi:10.1146/annurev-physiol-021014-071753

Ishihara, H., Martin, B. L., Brautigan, D. L., Karaki, H., Ozaki, H., Kato, Y., Fusetani, N., Watabe, S., Hashimoto, K., Uemura, D. et al. (1989). Calyculin A and okadaic acid: inhibitors of protein phosphatase activity. *Biochem. Biophys. Res. Commun.* **159**, 871-877. doi:10.1016/0006-291X(89)92189-X

Junutula, J. R., Schonteich, E., Wilson, G. M., Peden, A. A., Scheller, R. H. and Prekeris, R. (2004). Molecular characterization of Rab11 interactions with members of the family of Rab11-interacting proteins. *J. Biol. Chem.* **279**, 33430-33437. doi:10.1074/jbc.M404633200

Jurado, S., Goswami, D., Zhang, Y., Molina, A. J., Sudhof, T. C. and Malenka, R. C. (2013). LTP requires a unique postsynaptic SNARE fusion machinery. *Neuron* **77**, 542-558. doi:10.1016/j.neuron.2012.11.029

Kessels, H. W. and Malinow, R. (2009). Synaptic AMPA receptor plasticity and behavior. *Neuron* **61**, 340-350. doi:10.1016/j.neuron.2009.01.015

Kinoshita, E., Kinoshita-Kikuta, E., Matsubara, M., Yamada, S., Nakamura, H., Shiro, Y., Aoki, Y., Okita, K. and Koike, T. (2008). Separation of phosphoprotein isotypes having the same number of phosphate groups using phosphate-affinity SDS-PAGE. *Proteomics* **8**, 2994-3003. doi:10.1002/pmic.200800243

Kobayashi, H. and Fukuda, M. (2013). Arf6, Rab11 and transferrin receptor define distinct populations of recycling endosomes. *Commun. Integr. Biol.* **6**, e25036. doi:10.4161/cib.25036

Kopec, C. D., Li, B., Wei, W., Boehm, J. and Malinow, R. (2006). Glutamate receptor exocytosis and spine enlargement during chemically induced long-term potentiation. *J. Neurosci.* **26**, 2000-2009. doi:10.1523/JNEUROSCI.3918-05.2006

Lapierre, L. A., Avant, K. M., Caldwell, C. M., Oztan, A., Apodaca, G., Knowles, B. C., Roland, J. T., Ducharme, N. A. and Goldenring, J. R. (2012). Phosphorylation of Rab11-FIP2 regulates polarity in MDCK cells. *Mol. Biol. Cell* **23**, 2302-2318. doi:10.1091/mbc.e11-08-0681

Lindsay, A. J. and McCaffrey, M. W. (2002). Rab11-FIP2 functions in transferrin recycling and associates with endosomal membranes via its COOH-terminal domain. *J. Biol. Chem.* **277**, 27193-27199. doi:10.1074/jbc.M200757200

Lisman, J., Yasuda, R. and Raghavachari, S. (2012). Mechanisms of CaMKII action in long-term potentiation. *Nat. Rev. Neurosci.* **13**, 169-182. doi:10.1038/nrn3192

Malenka, R. C. and Bear, M. F. (2004). LTP and LTD: an embarrassment of riches. *Neuron* **44**, 5-21. doi:10.1016/j.neuron.2004.09.012

Malinow, R., Hayashi, Y., Maletic-Savatic, M., Zaman, S. H., Poncer, J. C., Shi, S. H., Esteban, J. A., Osten, P. and Seidenman, K. (2010). Introduction of green fluorescent protein (GFP) into hippocampal neurons through viral infection. *Cold Spring Harb. Protoc.* **2010**, pdb.prot5406. doi:10.1101/pdb.prot5406

Matsuda, S., Miura, E., Matsuda, K., Kakegawa, W., Kohda, K., Watanabe, M. and Yuzaki, M. (2008). Accumulation of AMPA receptors in autophagosomes in neuronal axons lacking adaptor protein AP-4. *Neuron* **57**, 730-745. doi:10.1016/j.neuron.2008.02.012

Mignogna, M. L., Giannandrea, M., Gurgone, A., Fanelli, F., Raimondi, F., Mapelli, L., Bassani, S., Fang, H., Van Anken, E., Alessio, M. et al. (2015). The intellectual disability protein RAB39B selectively regulates GluA2 trafficking to determine synaptic AMPAR composition. *Nat. Commun.* **6**, 6504. doi:10.1038/ncomms7504

Muto, A., Aoki, Y. and Watanabe, S. (2007). Mouse Rab11-FIP4 regulates proliferation and differentiation of retinal progenitors in a Rab11-independent manner. *Dev. Dyn.* **236**, 214-225. doi:10.1002/dvdy.21009

Naslavsky, N., Rahajeng, J., Sharma, M., Jović, M. and Caplan, S. (2006). Interactions between EHD proteins and Rab11-FIP2: a role for EHD3 in early endosomal transport. *Mol. Biol. Cell* **17**, 163-177. doi:10.1091/mbc.e05-05-0466

Otmakhov, N., Khibnik, L., Otmakhova, N., Carpenter, S., Riahi, S., Asrican, B. and Lisman, J. (2004). Forskolin-induced LTP in the CA1 hippocampal region is

NMDA receptor dependent. *J. Neurophysiol.* **91**, 1955-1962. doi:10.1152/jn.00941.2003

Park, M., Penick, E. C., Edwards, J. G., Kauer, J. A. and Ehlers, M. D. (2004). Recycling endosomes supply AMPA receptors for LTP. *Science* **305**, 1972-1975. doi:10.1126/science.1102026

Park, M., Salgado, J. M., Ostroff, L., Helton, T. D., Robinson, C. G., Harris, K. M. and Ehlers, M. D. (2006). Plasticity-induced growth of dendritic spines by exocytic trafficking from recycling endosomes. *Neuron* **52**, 817-830. doi:10.1016/j.neuron.2006.09.040

Petrini, E. M., Lu, J., Cognet, L., Lounis, B., Ehlers, M. D. and Choquet, D. (2009). Endocytic trafficking and recycling maintain a pool of mobile surface AMPA receptors required for synaptic potentiation. *Neuron* **63**, 92-105. doi:10.1016/j.neuron.2009.05.025

Prekeris, R., Davies, J. M. and Scheller, R. H. (2001). Identification of a novel Rab11/25 binding domain present in Eferin and Rip proteins. *J. Biol. Chem.* **276**, 38966-38970. doi:10.1074/jbc.M106133200

Shi, S. H., Hayashi, Y., Petralia, R. S., Zaman, S. H., Wenthold, R. J., Svoboda, K. and Malinow, R. (1999). Rapid spine delivery and redistribution of AMPA receptors after synaptic NMDA receptor activation. *Science* **284**, 1811-1816. doi:10.1126/science.284.5421.1811

Thomas, G. M. and Huganir, R. L. (2004). MAPK cascade signalling and synaptic plasticity. *Nat. Rev. Neurosci.* **5**, 173-183. doi:10.1038/nrn1346

Wang, Z., Edwards, J. G., Riley, N., Provance, D. W., Jr, Karcher, R., Li, X.-D., Davison, I. G., Ikebe, M., Mercer, J. A., Kauer, J. A. et al. (2008). Myosin Vb mobilizes recycling endosomes and AMPA receptors for postsynaptic plasticity. *Cell* **135**, 535-548. doi:10.1016/j.cell.2008.09.057

Wei, J., Fain, S., Harrison, C., Feig, L. A. and Baleja, J. D. (2006). Molecular dissection of Rab11 binding from coiled-coil formation in the Rab11-FIP2 C-terminal domain. *Biochemistry* **45**, 6826-6834. doi:10.1021/bi052655o

Welsh, G. I., Leney, S. E., Lloyd-Lewis, B., Wherlock, M., Lindsay, A. J., McCaffrey, M. W. and Tavare, J. M. (2007). Rip11 is a Rab11- and AS160-RabGAP-binding protein required for insulin-stimulated glucose uptake in adipocytes. *J. Cell Sci.* **120**, 4197-4208. doi:10.1242/jcs.007310

Woolfrey, K. M. and Dell'Acqua, M. L. (2015). Coordination of protein phosphorylation and dephosphorylation in synaptic plasticity. *J. Biol. Chem.* **290**, 28604-28612. doi:10.1074/jbc.R115.657262

Zheng, N., Jeyifous, O., Munro, C., Montgomery, J. M. and Green, W. N. (2015). Synaptic activity regulates AMPA receptor trafficking through different recycling pathways. *eLife* **4**, e06878. doi:10.7554/eLife.06878